Review article **Open Access**

Kimberly A. Sablon, Andrei Sergeev*, Sina Najmaei and Madan Dubey

High-response hybrid quantum dots-2D conductor phototransistors: recent progress and perspectives

DOI 10.1515/nanoph-2016-0159
Received September 18, 2016; revised November 13, 2016; accepted November 25, 2016

Abstract: Having been inspired by the tremendous progress in material nanoscience and device nanoengineering, hybrid phototransistors combine solution processed colloidal semiconductor quantum dots (QDs) with graphene or two-dimensional (2D) semiconductor materials. Novel detectors demonstrate ultrahigh photoconductive gain, high and selective photoresponse, low noise, and very high responsivity in visible- and near-infrared ranges. The outstanding performance of phototransistors is primarily due to the strong, selective, and size tunable absorption of QDs and fast charge transfer in 2D high mobility conductors. However, the relatively small mobility of QD nanomaterials was a technological barrier, which limited the operating rate of devices. Very recent innovations in detector design and significant progress in QD ligand engineering provide effective tools for further qualitative improvements. This article reviews the recent progress in material science, nanophysics, and device engineering related to hybrid phototransistors. Detectors based on various QD nanomaterials and several 2D conductors are compared, and advantages and disadvantages of various nanomaterials for applications in hybrid phototransistors are identified. We also benchmark the experimental characteristics with model results that establish interrelations and tradeoffs between detector characteristics, such as responsivity, dark and noise currents, the photocarrier lifetime, response, and noise bandwidths. We have shown that the most recent phototransistors demonstrate performance limited by the fundamental generation recombination noise in high gain devices. Interrelation between the dynamic range of the detector and the detector sensitivity is discussed. The review is concluded with a brief discussion of the remaining challenges and possible significant improvements in the performance of hybrid phototransistors.

Keywords: quantum dots; two-dimensional; graphene; hybrid phototransistors; responsivity; photoconductive gain.

1 Introduction

Light matter interactions in two-dimensional (2D) materials have unveiled diverse optoelectronic properties in this subclass of nanomaterials for a plethora of applications including photovoltaics, light-emitting diodes, sensing, and photodetection [1]. In fact, graphene has become a very desirable material for broadband, ultrafast optoelectronic applications due to the absence of a bandgap, which enables broadband interactions with light and hence wideband transparency. Combined with its high mobility, graphene is a strong contender for applications requiring work-function tunable and transparent conductive electrodes [1–3]. As a photodetector, the 2D nature of graphene makes field effect Fermi level control an efficient tool for device operation [4]. However, although these unique capabilities have sparked interest, the limitation in light absorption is undoubtedly the most central roadblock in developing useful 2D material base photodetection systems [5]. Besides graphene, other layered structures such as semiconducting transition metal dichalcogenides (TMDs) offer several advantages because of their tunable bandgap, strong light matter interaction, transparency, and mechanical flexibility [6], making them appealing materials for electronic and optical devices. However, unlike graphene, the mobility is much lower in this class of 2D semiconductors.

Therefore, hybridized systems that incorporate the unique properties of graphene and 2D semiconductors

***Corresponding author: Andrei Sergeev,** Sensors and Electron Devices Directorate, U.S. Army Research Laboratory, 2800 Powder Mill Rd, Adephi, MD, USA, e-mail: podolsk37@gmail.com
Kimberly A. Sablon, Sina Najmaei and Madan Dubey: Sensors and Electron Devices Directorate, U.S. Army Research Laboratory, 2800 Powder Mill Rd, Adephi, MD, USA

with other complementary optical systems such as colloidal quantum dots (QDs) have gained much traction due to the vast advantages provided by this union [7, 8]. For instance, the controllable size and shape of QDs offer the ability to combine high and selective coupling to electromagnetic radiation while the high electric conductivities and efficient electrostatic gating of graphene make it an excellent conductive channel material. While a complete understanding of 2D-QD charge transfer process remains elusive, it is known that the appropriate choice of material to include ligand strategy, design of QD optical properties, and the 2D electronic properties itself plays a significant role in device operation [9].

In this review, we discuss the research progress and direction in graphene and semiconducting 2D material base optoelectronics and highlight the most unique attributes of hybrid systems. First, advancements in fabrication technologies with emphasis on interface interactions are discussed, followed by physical mechanisms of photoresponse and basic parameters of photodetectors comparing graphene with 2D semiconductors with emphasis on responsivity, sensitivity, operating rate, and characteristic power. We conclude with a critical discussion of the maturity, challenges, and future perspectives of hybrid photodetection systems.

2 Fabrication technologies

The key to achieving better hybrid 2D-0D devices consists of the fabrication of atomically thin 2D materials and the engineering of QD solids with low defect concentrations and efficient carrier transport. Therefore, this section will highlight recent progress in the fabrication of 2D materials such as graphene and the TMDs such as MoS_2 and WS_2, as well as the synthesis of QDs with emphasis on ligand strategy.

Many methods for synthesizing and transferring graphene and the TMDs have been developed and explored during the recent surge of intense research. The most common fabrication technique used for single-layer and multi-layer 2D materials includes exfoliation and epitaxial growth [7, 10, 11]. In general, the type of method employed depends on the size, uniformity, and specific isomeric structure required. Vapor-phase epitaxy methods such as molecular beam epitaxy (MBE) and metalorganic chemical vapor deposition (MOCVD) are frequently used for wafer-scale growth of atomically precise heterojunctions of TMDs with good control of chemical composition, thickness, and uniformity [12]. With vapor-phase chemical reactions such as CVD, high-quality graphene films with large domains can be obtained. Nonetheless, although some reports claim that the thickness can be controlled, there are still a lot of uncertainties [13]. Furthermore, as the CVD growth of graphene strongly depends on the type of substrate employed, it is difficult to achieve separation without damage to the structure [13]. This challenge has direct technological impact on the development of roll-to-roll production of graphene as the intrinsic properties of graphene change in the context of contact electrode as a result of this step [14]. Simple inexpensive chemical and mechanical exfoliation techniques remain the most favorable methods for fabrication graphene structures. Mechanical exfoliation techniques typically result in small size and randomly distributed and oriented sheets on the substrate, which poses a significant challenge to device fabrication in the context of uniformity [15]. Figure 1A–D shows TEM images of resulting films from exfoliation and vapor phase epitaxy of MoS_2 and MoS_2/WS_2 hybrids. On the other hand, liquid exfoliation techniques, which include ion intercalation, ion exchange, and sonication-assisted exfoliation, are scalable and result in large quantities of nanosheets that can easily be dispersed into uniform films [15].

The hybridization of graphene and the TMDs with colloidal QDs can be achieved via assembly [19] or in situ methods [20]. The layer-by-layer (LbL) assembly method is most commonly used and relies on the electrostatic interaction of oppositely charged films [19]. LbL involves synthesis of separate components, which are then assembled through repeated drop-casting/spin-coating of graphene/TMDs and QDs successively on a highly doped or undoped substrate [16, 21–23] depending on the device configuration of choice [24]. Figure 2 illustrates QD-bottom and graphene-bottom hybrid transistors fabricated using this method. Various modifications of CVD techniques are employed to fabricate high-quality 2D conductors, such as graphene, MoS_2–WS_2 [18].

Colloidal QDs typically used for hybrid 2D-0D devices are made of PbS [7, 21–23], PbSe [26, 27], or ZnO [28] QDs. PbS/PbSe QDs are generally fabricated using wet chemical synthesis methods [7, 21–23, 26–29] that include thermal decomposition of organometallic precursors in the presence of a coordinating solvent, which provides a micelle-like ligand shell that controls the growth of the particles while ZnO QDs are grown using hydrothermal techniques [28]. The most important component of a hybrid phototransistor is the chemical structure, length, and conductivity of the ligands used during the synthesis of the QDs. As surface defects/traps can easily be introduced during the synthesis process, capping ligands are

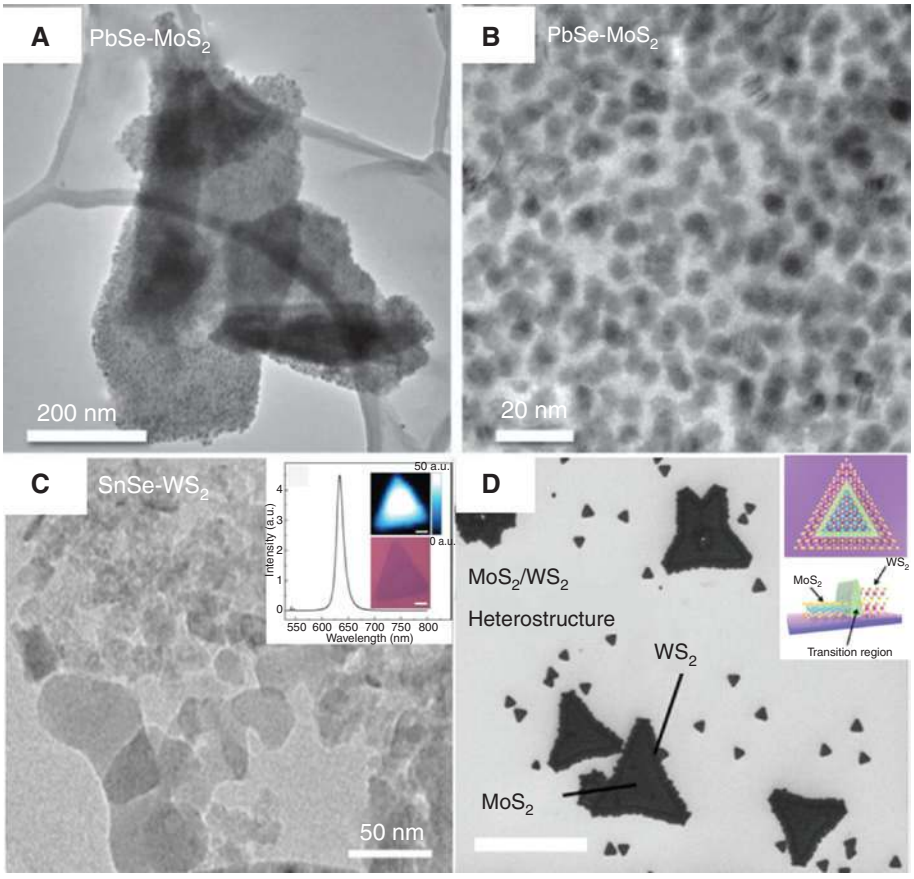

Figure 1: (A) TEM image of epitaxially grown PbSe-MoS_2; (B) HRTEM image of the PbSe-MoS_2 hybrid material showing the average size of 5.7 nm of the PbSe QDs, corresponding to a band gap of 0.74 eV; absorption edge of 1675 nm [16]. (C) TEM image of WS_2 grown by CVD Inset: Photoluminescence and PL mapping of a triangular WS_2 monolayer. The scale bar indicates 5 μm [17]. (D) SEM image of CVD grown heterostructure crystals. Scale bar: 30 μm. Inset: schematic of WS_2/MoS_2 in-plane heterojunctions [18].

used to passivate the surface of the QDs. However, these capping ligands ultimately determine the interparticle spacing between the QDs themselves and energetic barrier to charge transport at the QD-2D interface [26, 27, 29]. In general, capping ligands such as trioctylphosphine (TOP) and oleic acid (OA) are typically employed in the synthesis to reduce defect density, stabilize the QDs in solution by giving them a hydrophilic or hydrophobic surface, and prevent particle aggregation and precipitation [30, 31]. However, these long ligands create strong insulating barriers between QDs, reduce the coupling and hopping rate, and impede efficient carrier transport between the QD and the 2D material [26, 27, 29].

Ligand exchange processes are commonly used to replace the long-chain ligand with small molecules such as amines [32], thiols [33–35], and hydrazine [36]. However, it can be difficult to stabilize QDs such as PbS and PbSe using short surfactant ligands, as both size and shape of the dots can be compromised during the exchange process [35–41]. In their work on QD solids, Jeong et al. demonstrated complete removal of oleic acid on PbS QDs using ethanedithiol (EDT) and mercaptocarboxylic acids (MPA) treatments to fabricate QD solids with enhanced mobility and lifetime [33]. Meanwhile, Talapin et al. completely removed the oleic acid on PbSe QDs with diluted hydrazine to fabricate phototransistors with high conductivities [35]. Turyanska et al. also demonstrated significant enhancement in conductivity using short thiol-based ligands of thioglycerol/dithioglycerol or polyethylene glycol [36]. On the other hand, to achieve better control over the stoichiometry of the QDs during ligand exchange processes, Zhang et al. demonstrated the use of a metal-free chalcogenide compound, $(NH_4)S_2$, to remove bulky surfactant ligands [37]. This treatment differs significantly from others employing thiols, halides, and carboxylates because it creates inorganically interconnected QD solids through metal-sulfide bonds resulting in a significant decrease in the interparticle spacing. Table 1 summarizes commonly used ligand anchors groups with information on length, mobility, lifetimes, and corresponding

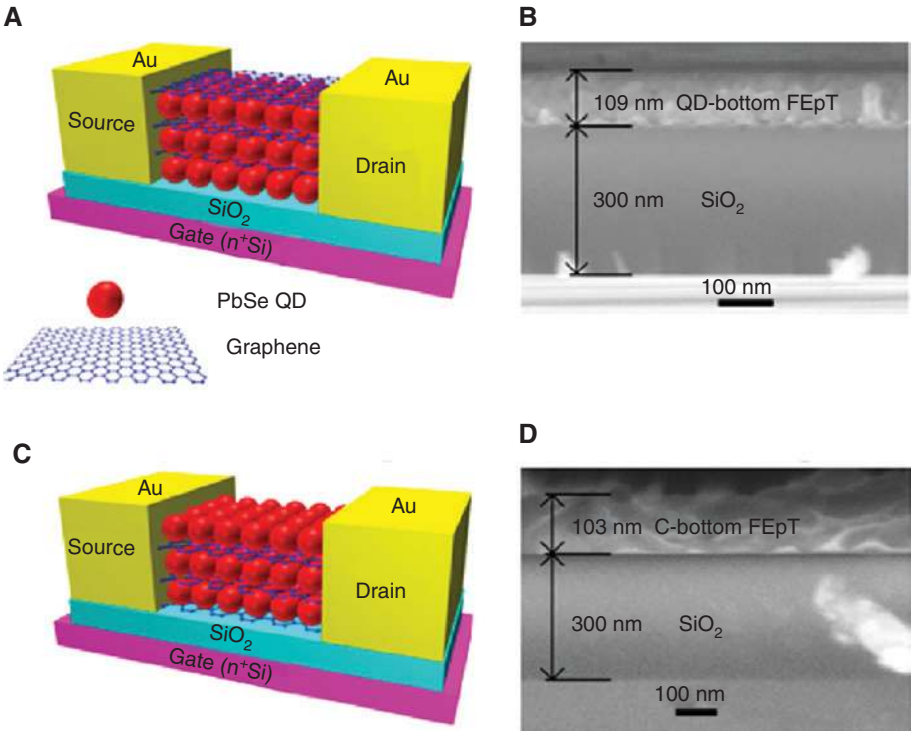

Figure 2: (A) Schematic illustration of the QD-bottom phototransistor; (C) the G-bottom phototransistor on a Si n+/SiO_2 substrate. Cross-sectional SEM images of the channel in the QD-bottom phototransistor (B) and the G-bottom phototransistor (D) [25].

diffusion coefficient, which exponentially decreases with the increase of the ligand length.

3 Photodetectors: main characteristics and tradeoffs

This section briefly highlights the main parameters of photodetectors and tradeoffs in sensing technologies. In the context of photodiodes and phototransistors, our discussion and consideration are limited to detectors based on the phenomena of photoconductivity. It is convenient to separate light-induced generation, which provides photocarriers to the transistor channel, and capture/recombination processes, which remove photocarriers from the channel. The external quantum efficiency (EQE), η, is defined as the probability that the incoming photon creates a unit charge carrier in the channel. The perfect readout does not affect photocarriers. The photocarrier may be captured or recombined upon return from the readout circuit to the photoconductor. The probability

Table 1: Properties of ligands.

Capping ligands	Length Å	Mobility $cm^2/V{\cdot}s$	Lifetime (s)	Diffusion coefficient cm^2/s	Ref.
Hydrazine	–	1	–	0.026	[33]
Oxalic acid	3.5	0.41	$<5\times10^{-9}$	0.01	[26]
1,2-Ethanediamine	3.8	1.6	1.25×10^{-8}	0.041	[26]
1,2-Ethanedithiol	4.1	0.07	–	1.8×10^{-4}	[24]
		2.4×10^{-4}	9.3×10^{-6}	6.2×10^{-6}	[31]
3-Mercaptopropionic acid	5.0	5.1×10^{-3}	3.1×10^{-5}	1.3×10^{-4}	[31]
1,3-Propanedithiol	5.5	4.0×10^{-3}	–	10^{-4}	[24]
1,4-Butanedithiol	6.8	7.0×10^{-3}	–	1.8×10^{-4}	[24]
1,5-Pentanedithiol	8.0	3.0×10^{-4}	–	0.8×10^{-5}	[24]
1,6-Hexanedithiol	9.8	7.0×10^{-4}	–	1.8×10^{-5}	[24]

of this process is given by the ratio of the transit time, τ_{tr}, which the photocarrier spends in the photoconductor, to the photocarrier lifetime, τ_ℓ. The photoconductive gain, $\gamma = \tau_\ell/\tau_{tr}$, refers to the number of times the photoelectron can circulate in the readout circuit. With these two dimensionless parameters, η and γ, that describe the photocarrier generation and recombination processes, the photocurrent may be presented as $J_{ph} = e\eta\gamma P/(h\nu)$ where e is the unit charge, P is the electromagnetic power, and $h\nu$ is the energy of a photon. Thus, the responsivity of the photodetector is given by

$$R \equiv \frac{J_{ph}}{P} = \frac{e\eta\tau_\ell}{h\nu\tau_{tr}} = \frac{e\eta\gamma}{h\nu}. \quad (1)$$

Let us highlight that these simple equations for the photocurrent and responsivity are only applicable to the non-degenerate photoconductors.

It is convenient to present EQE as a product of the absorption coefficient $\alpha(\nu)$ and internal quantum efficiency (IQE), η_{int}, i.e. $\eta = \alpha(\nu)\cdot\eta_{int}$. The detector operating time is τ_ℓ, and the corresponding electronic bandwidth, i.e. operating rate, $B = 1/(2\tau_\ell)$. Long photocarrier lifetime increases the responsivity but decreases the operating rate.

The detector sensitivity is determined by the signal-to-noise ratio. To present the noise current in the photoconductor, let us assume that without light, there are N_{th} thermally excited charge carriers in the channel. Then, the dark current is given by $J_{dc} = eN_{th}/\tau_{tr}$. Thermal fluctuations in N_{th} lead to the generation-recombination (GR) noise current. Taking into account that the average fluctuation of N_{th} is $N_{th}^{1/2}$ and the noise bandwidth of GR processes, $B = (2\tau_\ell)^{-1}$, the GR noise current is given by

$$J_{GR} = \frac{e\sqrt{2N_{th}}}{\tau_{tr}}\frac{1}{\sqrt{B}} = 2\sqrt{eJ_{dc}\gamma}. \quad (2)$$

Another source of the noise current is the shot noise, which is determined by the total current, i.e. the sum of the dark current and the photocurrent,

$$J_S = 2\sqrt{e(J_{dc} + J_{ph})}. \quad (3)$$

The total noise current, J_{noise}, is equal to $(J_{GR}^2 + J_S^2)^{1/2}$. The sensitivity of the detector is characterized by the noise equivalent power: $NEP = J_{noise}/R$, which is proportional to the square root of the photoconductor volume. The detectivity, D^*, is used to characterize the optoelectronic material or structure. It is defined as $D^* \equiv \sqrt{S}/NEP = \sqrt{S}R/J_{noise}$, where $S = L\times W$ is the photodetector square. In the case of small photon fluxes, when the photocurrent is much smaller than the dark current, the detectivity is given by

$$D^* = \frac{\eta}{2h\nu}\sqrt{\frac{e\cdot S}{J_{dc}}}\cdot\sqrt{\gamma}. \quad (4)$$

Thus, the high photoconductive gain improves both the detector responsivity and sensitivity (NEP and detectivity). To achieve high photoconductive gain, $\gamma = \tau_\ell/\tau_{tr}$, as well as high device operating rate, $1/\tau_\ell$, one should decrease the transit time, $\tau_{tr} = L/\mu E$, i.e. increase the photocarrier mobility, μ. As the intensity of thermodynamics calculations increases as a square root of the photoconductor thickness, the low dimensional materials are favorable for sensing. Therefore, the 2D materials are expected to greatly impact detector technologies. However, as mentioned earlier, perfect 2D materials cannot provide effective absorption of electromagnetic radiation. Therefore, it makes sense to combine such materials with QDs, which show effective resonant absorption via the light-induced electron transitions in dots. Finally, we would like to note that the consideration above and all corresponding equations are applicable to the non-degenerate conductors (semiconductors). The photoresponse of weakly degenerate graphene will be discussed in Section 5.2.

4 Optoelectronic properties of colloidal QDs

Colloidal QD photodetectors have attracted intense attention during the last decade because of their low processing cost and unique optical properties. Solution processed QD nanomaterials combine high and selective coupling to electromagnetic radiation, impressive photoconductive gain, and high photoconductivity [38, 39]. QD photodiodes demonstrate substantial photoresponse in visible-, near-infrared (NIR), and short-wavelength infrared (SWIR) ranges. The photoresponse spectrum is determined by the QD electron level spacing, which can be controlled by the dot size and shape [40]. As an example, Figure 3 demonstrates the bandgap of PbSQDs as a function of quantum diameter, d, [41]. According to the theory [40], the bandgap in spherical QDs is given by

$$E_g^{QD} = E_g^{bulk} + \frac{2h^2}{d^2}\left(\frac{1}{m_e} + \frac{1}{m_h}\right) - \frac{3.6e^2}{4\pi\varepsilon\varepsilon_0 d}. \quad (5)$$

Comparing the experimental curve with Eq. 5, we see that in the nanoscale range of nanoparticle diameters,

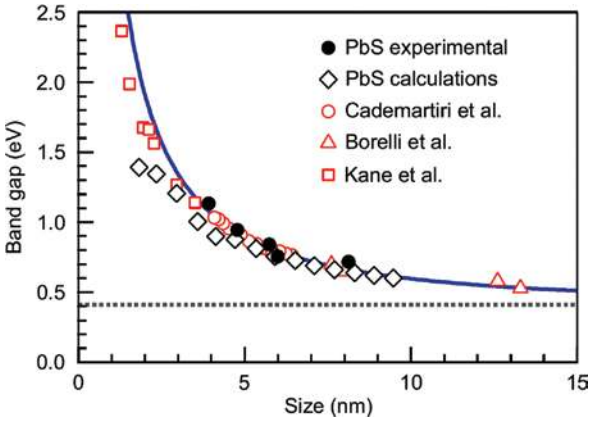

Figure 3: Effect of QD size on the bandgap of PbS QDs [41].

both the confinement effect (the second term in Eq. 5) and the Coulomb interaction (the third term in Eq. 5) determine the bandgap in the spectrum of nanoparticles.

The analogous dependencies for the QD bandgap vs. QD size were observed for PbSe and ZnO nanoparticles [42–44]. Thus, for variety of QDs, quantum confinement provides wide spectral tunability within a single QD material.

Carriers trapped in QDs very effectively interact with electromagnetic radiation via radiative excitation and recombination (relaxation) processes [45–47]. If other interactions are weak, the radiative processes lead to strong resonance light scattering by QDs with negligible absorption. The absorption processes are realized due to radiative electron transition to QD excited states and nonradiative recombination and escape processes, when excited photocarriers escape to QD surface traps or transfer to conducting states in the matrix and contribute to the photocurrent. The scattering and absorption processes may be described by the radiative, γ_r, and nonradiative, γ_{nr}, damping coefficients. The corresponding resonance scattering and absorption cross-sections of QDs as functions of the light frequency ($\omega = 2\pi\nu$ and $\lambda = c\nu$) are given by Ref. [48]

$$\sigma_{sc} = \frac{3\lambda^2}{2\pi} \frac{\gamma_r^2/4}{(\omega_0 + \Delta\omega - \omega)^2 + (\gamma_r + \gamma_{nr})^2/4}, \tag{6}$$

$$\sigma_{abs} = \frac{3\lambda^2}{2\pi} \frac{\gamma_r \gamma_{nr}/4}{(\omega_0 + \Delta\omega - \omega)^2 + (\gamma_r + \gamma_{nr})^2/4}, \tag{7}$$

where ω_0 is the resonance frequency of electron transitions in QDs and $\Delta\omega$ is its exciton energy correction. Thus, the ratio of absorption cross-section to the scattering cross-section is γ_{nr}/γ_r. Near the resonance, the absorption cross-sections have a wide maximum at $\gamma_{nr}=\gamma_r$, and the corresponding cross-sections at $\gamma_{nr}=\gamma_r$ are as follows:

$$\sigma_{abs} = \sigma_{sc} = \frac{3}{8\pi}\lambda^2. \tag{8}$$

Therefore, for optimization of QD optoelectronic devices, it is critically important to enhance the resonance absorption and scattering. The scattering processes strongly increase light trapping and allow for reduction of the absorber thickness by $4n^2$ times, where n is the refractive index of the QD material [49, 50].

The equations above relate the absorption in QDs to the photocarrier kinetics. To provide the resonance absorption in QDs and simultaneously minimize the emission losses, the characteristic time of the photocarrier transfer from QD excited states to conducting states should be 3–5 shorter than the radiative recombination time in QDs.

Quantum confinement in QD nanomaterials also strongly modifies the relaxation and recombination processes. Electron-phonon relaxation is suppressed when the energy level spacing exceeds the characteristic phonon energies, while the electron-electron (hole) interaction is enhanced. Strong interaction between electrons and holes leads to multiple exciton generation (MEG) [51], which may increase the quantum efficiency above 100% [52, 53]. Strong resonance absorption and high quantum efficiency result in significant responsivity, R, which may exceed 10^3 A/W in QD photodiodes. Relatively low levels of the generation-recombination noise and transport noise lead to an impressive signal-to-noise ratio and the corresponding detectivity of 10^{13}W/Hz$^{1/2}$ (Jones) [54, 55].

Compared with perfect crystalline semiconductors, the colloidal QD materials are strongly nonhomogeneous at the nanoscale level. Spatial fluctuations in the material structure produce significant nanoscale potential profile, which drastically affect both transport and kinetic phenomena. The negative effect of this nanoscale profile is the significant mobility suppression due to photocarrier scattering from the random profile, from ~100 cm^2/Vs in crystalline materials to 10^{-5}–10^{-1} cm^2/Vs in colloidal QDs. The positive effect of this profile is the nanoscale separation of electron and holes, which substantially increases the photocarrier lifetime, up to several microseconds. Thus, both characteristic transport (transit) and recombination times strongly increase in colloidal QD devices. Such photocarrier kinetics provides a high photoconductive gain compared with that of MBE grown QD structures but significantly decreases the device operating rate. Therefore, significant technological efforts were aimed at

passivation of shallow photoelectron traps. Recent results demonstrate very significant improvement in the photocarrier mobility, which, in turn, reduces the PbSe QD photodiode operating time to 74 ps [39].

5 Hybrid QD-2D conductor phototransistors

Use of high mobility 2D conductors in photodetectors can significantly decrease the transit time during which photocarriers leave the photoconductor. This, in turn, increases the photoconductive gain, photoresponse, and detectivity of detectors (Eqs. 1 and 4). However, pure 2D materials demonstrate weak interactions with the electromagnetic radiation because the Drude absorption in this case is negligible and band-to-band absorption is small due to the ultra-thin thickness. For example, graphene with a photocarrier mobility of $\sim 10^4$ cm^2/Vs, which is one–two orders of magnitude higher than the mobility in crystalline silicon, absorbs just 2% of incoming electromagnetic radiation. As we discussed in the previous section, colloidal QD nanomaterials are low-cost selective and tunable absorbers, which provide effective conversion of photons into electron-hole pairs. Therefore, the combination of QDs and graphene into optoelectronic nanomaterial is very promising for detector technologies.

The phototransistor is the simplest detector, where light absorption and carrier collection are realized in different parts of photodetector and these key functionalities may be optimized independently. Modern field-effect phototransistors demonstrate the gain values of 10^2–10^3 with the operating bandwidth of $\sim 10^6$ Hz [56, 57]. In phototransistor, the electron-hole pairs are generated in the gate volume and may be transferred via thermionic or tunneling effects to the high-mobility source-drain channel. Tuning the gate voltage allows one to realize conditions at which the electron and hole transfer processes are substantially asymmetric. One type of photocarriers mainly moves to the channel, while another type of carrier is predominantly trapped in the gate volume. The photocarrier lifetime is limited by capture processes from the channel to the gate and typically the lifetime strongly exceeds the recombination time in the channel. Finally, high mobility and long photocarrier lifetime lead to large values of the photoconductive gain.

Let us note that modern MBE grown QD nanomaterials also provide high mobility along with selective and controllable absorption. The MBE grown QD IR photodetectors (QDIPs) as well as quantum well IR photodetectors (QWIPs) are usually based on inter-subband electron transitions. Due to high mobility and relatively large photoelectron capture time, the MBE grown QDIPs demonstrate very high gain [58, 59]. The main drawback of MBE grown QD structures is a small absorption coefficient. Doping of QDs enhances inter-subband electron transitions and increases the absorption coefficient but simultaneously increases the dark current and noise current. For these reasons, the operation of MBE grown QD infrared photodetectors is limited by temperatures of 70–120 K [60].

The hybrid phototransistor is a detector of choice to combine QD absorber with 2D conducting channel. During the last decade, significant scientific and engineering investigations were aimed at the development of hybrid graphene-QD structures with high electron coupling between these two components (see Figure 2). The first operation of hybrid QD-graphene phototransistor has been demonstrated in Ref. [7]. Konstantatos and coworkers sensitized PbS QDs with the first exciton peak at 950 nm and 1450 nm and deposited colloid QDs on graphene flakes, which were prepared by standard mechanical exfoliation. The hybrid transistor demonstrated a photoconductive gain of 10^8, responsivity of 10^7 A/W, and detectivity of 7×10^{13} Jones with the signal rise and relaxation times of ~ 10 ms. This work has attracted significant attention to hybrid QD-2D conductor transistors. Devices having a graphene channel and PbS QDs were also investigated in Refs. [10, 61–63]. In other works, the graphene channel was combined with ZnO QDs [28, 64] and recently with PbSe QDs [25, 65]. Besides graphene, MoS_2, WS_2, and SnS_2 were investigated as possible 2D conductors for the source-drain channel. Phototransistors with PbSe QDs on MoS_2 nanosheets were studied in Ref. [16]. SnSe nanocrystals were combined with WS_2 monolayer in Ref. [17]. Copper indium sulfide QDs deposited on SnS_2 were studied in Ref. [8]. Advanced MoS_2 phototransistor [66] was combined with PbSQD nanomaterial in Ref. [21]. Dependence of the photoresponse of hybrid transistors on QD functionalization (capping with various ligands) was investigated in Refs. [36] and [67]. All hybrid phototransistors demonstrated high gain, responsivity, and detectivity but relatively long rise and relaxation times, which changes from several subseconds to dozens of seconds. To accelerate charge transfer between QDs and 2D conductors, in a very recent work [68], Nikitskiy et al. employed the device architecture [69] that combines the QD photodiode with transistor.

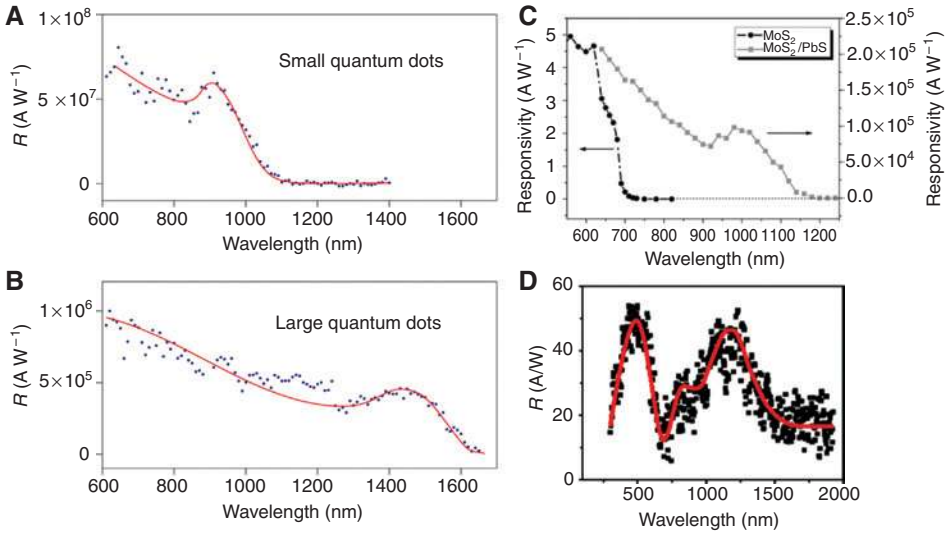

Figure 4: Spectral characteristics of various hybrid phototransistors: (A) and (B) graphene devices with small and large PbS QDs [7], (C) MoS_2 device with PbS QDs [21], and (D) graphene device with PbSe QDs [65].

5.1 Spectral characteristics and responsivities

In Figure 4, we present the spectral responsivities of hybrid phototransistors with various QD nanomaterials. Let us highlight that without QDs, the photoresponse of transistors is negligible, because the absorption of monolayers is very small. In the case of graphene channel, the direct photoresponse is also strongly suppressed by strong recombination processes with picosecond characteristic time. Thus, in all devices, the photoresponse originates from the light-induced exciton generation in QD structures and the spectral photoresponse characteristics correlate well with the absorption of QDs.

In Ref. [7], the authors investigate two phototransistors with graphene channel and PbS QDs of different sizes with the first exciton peaks at 950 nm and 1450 nm. Figures 4A and B show that spectral photoresponse follows the absorption of PbS QDs. Figure 4C demonstrates the spectral photoresponse of PbS QDs deposited on MoS_2 [21]. The MoS_2 transistor without QD structures shows negligible photoresponse in the wavelength range above 700 nm. Addition of QD nanomaterial increases the photoresponse by five orders of magnitude and shifts its spectral boundary to ~1150 nm. The spectrum of the photoresponse correlates well with PbS absorption with a exciton peak at 980 nm. Figure 4D presents the spectral photoresponse of the phototransistor with MEH-PPV/PbSe nanomaterial integrated with monolayer graphene, where MEH-PPV is the polymer 2-methoxy-5-(20-ethylhexyloxy-p-phenylenevinylene) [65]. The photoresponse spectrum shows two distinct peaks, which originate due to absorption in PbSe QDs (the long wavelength peak) and MEH-PPV (the short wavelength peak). In Ref. [68], the PbS colloidal QDs with the exciton peak at 1600 nm allows for extending operation of ITO-QDs-graphene diode-transistor photodetector to 1700–1800-nm wavelength (0.7 eV or 170 THz). Thus, spectral responsivities of hybrid phototransistors are determined by the absorption spectra of QD nanomaterials and can be controlled by QD size.

The characteristics of phototransistors measured in the most of the reports discussed are summarized in Table 2. Practically all of the hybrid devices demonstrate very high responsivity, up to 10^7 A/W. Due to such high responsivities, the phototransistors do not require any amplifiers. Figure 5 shows that the responsivity is proportional to the drain-source voltage, V_{ds}, in the wide range of V_{ds} [10, 17]. This dependence is highly expected because the transit time is inversely proportional to V_{ds}, and therefore, the photoconductive gain is proportional to V_{ds}, i.e.

$$\gamma = \frac{\tau_\ell}{\tau_{tr}} = \tau_\ell \frac{\mu V_{ds}}{L^2}, \tag{9}$$

where L is the channel length (see Table 2).

5.2 Transient photoresponse, photocarrier lifetimes, and photoconductive gain

The transient photoresponse was measured in most of the reports on hybrid phototransistors. The characteristic

Table 2: Characteristics of hybrid phototransistors.

QDs-2D channel	QD capping	Responsivity (A/W)	Rise time (s)	Fall time (s)	β $R \propto P^{-1+\beta}$	QD layer thickness (nm)	Channel length (μm)	Ref.
PbS QDs-Graphene	Ethanedithiol	5×10^{7}	0.01, 1	0.01, 2	0	80	10	[7]
PbS QDs-Graphene	Pyridine	$\sim10^{7}$	0.13, 5	0.25, 5	0.24	45–250	1	[10]
PbS QDs-Graphene	Default	2.8×10^{3}	~1	~10	–	1–5	3	[61]
PbS QDs-Graphene		2×10^{5}	0.7, 4.5	1.8, 7.9	0	–	–	[23]
ZnO QDs-Graphene		10^{4}	–	5	0	Several tens	10	[28]
PbSe QDs-Graphene		~1	0.7, 2.4	0.7	–	3 QD layers	100	[25]
PbSe QDs-Graphene		130	~10	~10	0	–	100	[65]
PbSe QDs-MoS_2	Oleic acid	–	0.25	0.43	–	QD islands	5	[16]
PbS QDs-WS_2		0.007	0.0082	0.0084	0.45–0.69	QD islands	–	[17]
$CuInS_2$ QDs-SnS_2	Ethanedithiol	630	~0.1	~0.1	0.48	~One layer	–	[8]
PbS QDs-MoS_2	Ethanedithiol	6×10^{5}	~0.1	0.3–0.4	~0.3	40–60	12	[21]
PbS QD-Graphene	Thioglycerol	10^{9}	10^{-3}, 1	10^{-3}, 1	0	–	6	[36]
PbSe QDs-Graphene Nanomech	Trioctylphosphine (TGO)	1800	0.015	–		AAO mask	200	[67]
	Oleic acid (OA)	34	0.035	–			200	
	Pyridine	1760	0.64	–			200	
	PANY: TOPO + aniline tetramer	574	>1	–			200	
ITO-PbS QDs-Graphene		10^{6}	$\sim10^{-4}$	$\sim10^{-4}$	0	300	10	[68]

times obtained in these measurements are summarized in Table 2. Detailed studies of graphene-QDs phototransistors have shown that the increase of photocurrent with the illumination and its decrease when the light is switched off are well described by bi-exponential dependencies with two characteristic times (see Figure 6). The longer time changes from ~1 to 10 s, and the short time changes from 0.01 to 1 s. The rise and fall transient characteristics turn out to be rather symmetric, i.e. the characteristic rise and relaxation times in a particular device are very close. The decay (rise) of photocurrent with two distinct characteristic times was associated with the multiplicity photocarrier traps at the surface of the QDs [7] or with slow electron and fast hole processes [10].

Photoconductive gain may be evaluated as a ratio of the photocarrier lifetime to the transit time (Eq. 9). The product of EQE and the gain can be determined from the responsivity (Eq. 1). Using the data of Ref. [7], we find that at maximal responsivity, $R=4\times10^{7}$ A/V, which is obtained under a laser illumination with $\lambda=532$ nm and at the drain-source voltage $V_{dc}=5$V, the EQE-gain product is $\eta\gamma=Rh\nu/e\approx10^{8}$. Based on the extracted mobility of 1×10^{3} cm^2/Vs, we find the transit time of ~0.2 ns. Evaluating the gain via photoelectron lifetime, we obtain $\sim5\times10^{9}$ for the 1-s lifetime, which corresponds to the long relaxation time observed in the transient photoresponse. Then, calculating EQE, we get $\eta\approx0.02$. In QD-graphene phototransistors, EQE is the product of probabilities of several processes, which include the photon absorption in QDs, photocarrier extraction from QD to matrix, and finally the charge transfer from QD structures to graphene. As the light-induced charge transfer, ΔQ, also results in the shift of gate voltage, ΔV_g, which is interrelated via the gate-channel capacitance, $\Delta Q=C_{gc}\Delta V_g$. Then, the external quantum efficiency related to the photon-charge carrier conversion may be presented as follows:

$$\eta^{*}=\frac{C_{gc}\,\Delta V_{g}}{e\tau_{\ell}\,\Delta P/h\nu}. \tag{10}$$

According to Ref. [7], the power of 0.1 pW induced a 2-V gate shift, and the capacitive coupling C_{gc}/e was $\sim7\times10^{10}$ $cm^{-2}\,V^{-1}$, which leads to a EQE of ~0.25 [7].

The accurate evaluations show that the quantum efficiency, $\eta\sim0.02$, determined from the responsivity (i.e. photocurrent) is substantially below the efficiency of the photon to charge carrier conversion, $\eta^{*}\sim0.25$. This significant difference has a simple explanation. These two quantum efficiencies should coincide only in the non-degenerate conductors, because Eq. 1 is not applicable to the degenerate photoconductor. The photoelectron placed

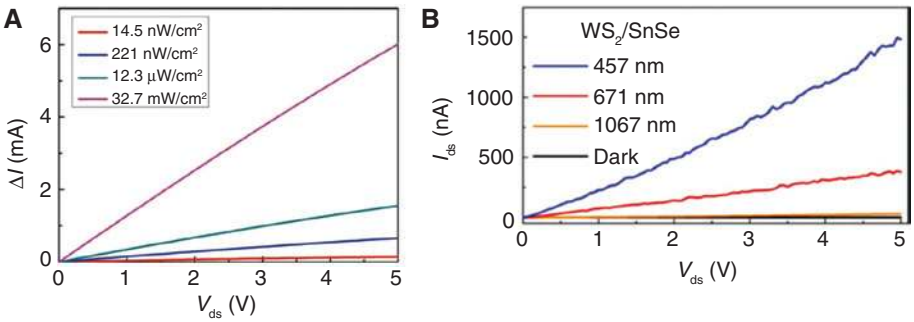

Figure 5: Photocurrent as a function of the drain-source voltage at various EM powers: (A) the graphene transistor with PbS QDs [10] and (B) the WS_2 transistor with PbS QDs [17].

at the Fermi surface of the degenerate conductor contributes to the photocurrent via the shift of the Fermi energy and the corresponding increase of electron density of states at the Fermi level. In the degenerate conductor, the efficiencies discussed are related by

$$\eta \approx \frac{kT}{\varepsilon_F} \cdot \eta^*. \tag{11}$$

Thus, intentional or unintentional doping of graphene substantially reduces the quantum efficiency.

As seen from Table 2, practically all hybrid phototransistor were fabricated with short (micron) high-mobility 2D channels that provide high gain. The photoresponse in these devices may decrease due to the small efficiency of charge transfer via the QD structure-channel interface as well as due to doping of the channel, including unintentional doping due to the charge transfer from QDs to the channel without light. Let us also note that doping of the channel also increases the dark current and noise.

5.3 Polarity of photoresponse

In both materials, graphene and the QD structures, the electric charge may be transferred by electrons as well as by holes. Which light-induced carriers are injected from QDs to graphene? According to Ref. [7], the sign of injected photocarriers depends on graphene doping. In the

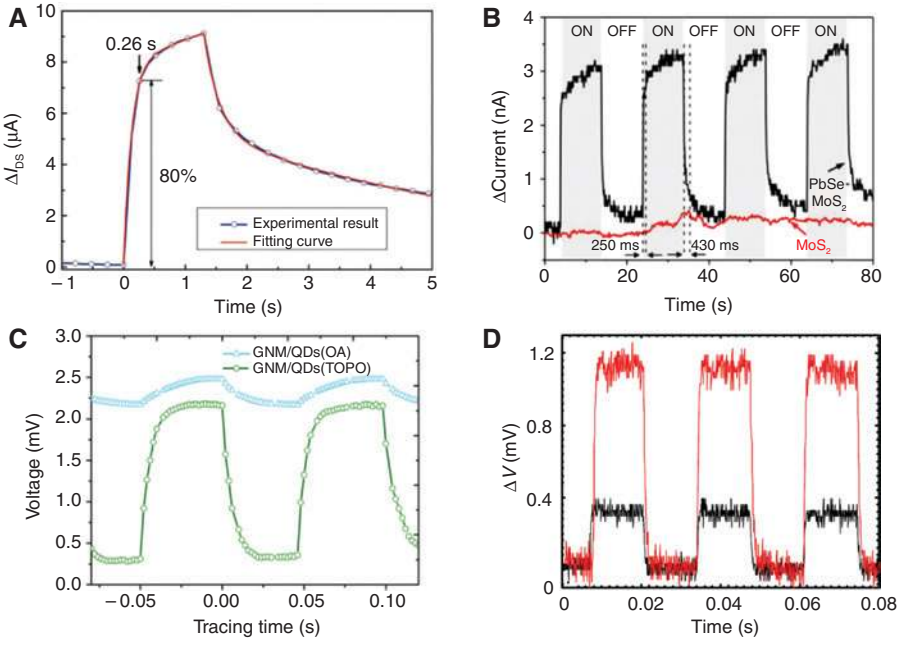

Figure 6: Transient photoresponse: (A) the graphene transistor with PbS QDs [10], (B) the MoS_2 transistor with PbS QDs [16], (C) the graphene nanomech transistor with PbSe QDs [67], and (D) integrating diode-transistor detector based on graphene with PbS QDs [68].

undoped graphene with the work function of ~4.5–4.6 eV, the chemical potential (i.e. the Dirac point) is slightly above the chemical potential of the p-doped PbS QD nanomaterial with the work function of ~4.9 eV. Therefore, in the absence of light, the charge is transferred from QDs to graphene. This charge transfer creates the electric field in the direction from graphene to the QDs. The photocarriers created in the QD structure are separated by this field and photoelectrons move from QDs to graphene, while holes are trapped in the QDs.

The charge motion is opposite, if the graphene is p-doped and the Fermi energy of holes exceeds 0.3–0.4 eV. In this case, the chemical potential of carriers in graphene turns out to be below the chemical potential of QDs, which leads to the charge transfer from graphene to QDs. The induced electric field forces photo-holes to move from QDs to graphene. In Ref. [7], the above model was confirmed by the measurements of the gate voltage shift due to the QD deposition and the light-induced shift. As it is shown in Figures 7A and B, the channel resistance as a function of the gate voltage reaches a maximum (the current has a minimum) when the electrochemical potential crosses the Dirac point. If the positive (negative) charge is transferred to the graphene, position of the Dirac voltage shifts to higher (lower) voltages. Let us note that the analogous shifts of the gate voltage due to QD deposition doping and light-induced doping of graphene were observed in Refs. [61] and [62]. The main conclusion of the model [7] is that because the light-induced process is realized due to the electric field created by QD deposition, the light-induced charge transfer (Dirac voltage) is opposite to the charge transfer related to QD deposition on graphene.

However, different results have been obtained in Ref. [10] (see Figures 7C and D). It was found that while the deposition of PbS QDs on graphene leads to the p-doping of graphene and corresponding positive shift of the Dirac point (~47 V), the light-induced shift of the gate voltage is in the same direction to higher voltages. In other words, the light also results in p-doping of graphene. Thus, the light-induced charge transfer is not completely controlled by the electric field between QDs and graphene.

As mentioned earlier, the QD capping ligands play a critical role in the charge transfer process. Turyanska et al. in Ref. [36] investigated PbS QDs of 4.5-nm diameter capped by polyethylene glycol H-(O-CH_2-CH_2)$_n$-OH with n=2000 (P2000) and n=500 (P500). The P2000 and P500 ligands have length of 10 nm and 5 nm correspondingly. They also studied QD capping with a mixture of thioglycerol (TGL) and dimercapto-propanol, which has a short length of ~0.5 nm. It was found that deposition of any of these three QD nanomaterials results in n-doping of graphene. A significant shift in the Dirac point was observed when the QD material with TGL capping was deposited. As expected, the photoresponse of the transistor with TGL QD material significantly exceeds the photoresponse of the device with P500 nanomaterial, which,

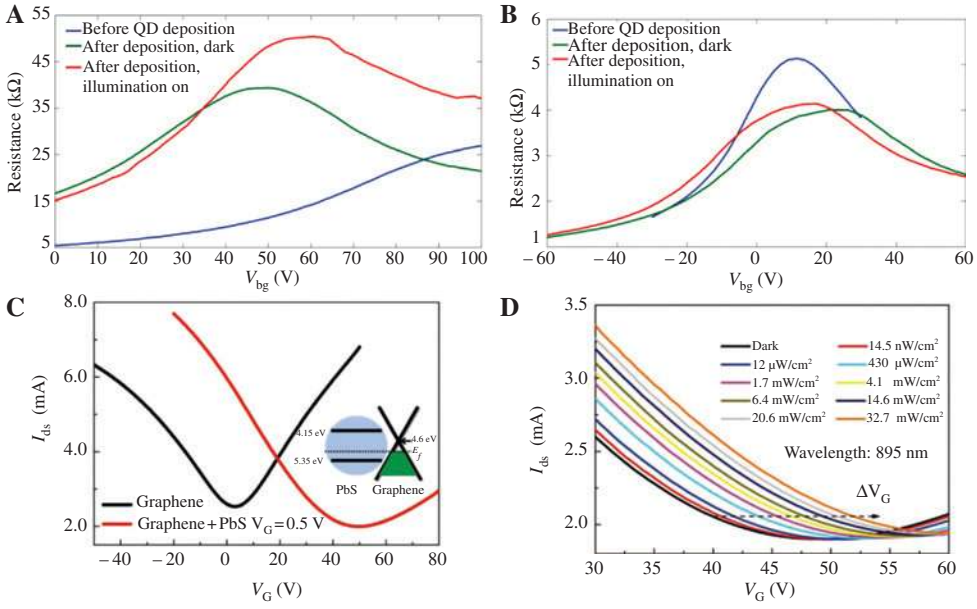

Figure 7: Shift of the gate voltage due to QD deposition and the light-induced shift of the gate voltage in the device with undoped graphene (A) and p-doped graphene (B) and PbS QDs [7]. (C) Gate voltage shift due to PbS QD deposition in graphene phototransistor and (D) the light-induced shift of the gate voltage [10].

in turn, shows substantially larger photoresponse than the device with P2000 nanomaterial. An interesting effect of light on the polarity of the graphene was observed. The presence of light results in the n-doping of graphene for the transistors with P500 and P2000 nanomaterial but leads to the p-doping of graphene in devices with TGL QD material (see Figure 8). Thus, the data of Ref. [36] show that only in the QD nanomaterial with short ligands is the light-induced charge transfer determined by the electric field created during the QD deposition.

Summarizing this section, let us highlight that the high photoconductive gain and responsivity are observed in hybrid transistors with high mobility graphene and MoS_2 channels. Decrease of mobility in the channel, for example, the graphene nanomesh channel, strongly reduces the responsivity. As it will be discussed in the next section, high photoresponse also requires strong electric coupling between the QD structure and the high mobility channel. The coupling increases in structures with short ligands (ethanedithiol and thioglycerol), which are used for QD capping.

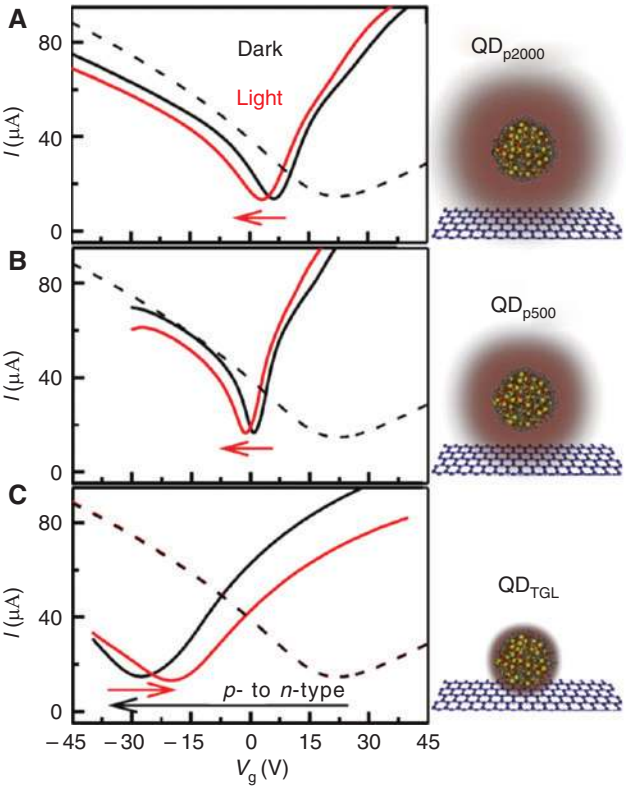

Figure 8: The gate voltage shift due to QD deposition (black solid lines) and the light induced shift (red lines) in graphene transistors with PbS QD nanomaterials with different ligands [36].

5.4 Photoreponse vs. electromagnetic power

The photoresponsivity of hybrid phototransistors demonstrates complex dependencies on the radiation power (see Figure 9). In Ref. [7], it was found that the responsivity does not change at low electromagnetic powers, up to 50 fW. At higher power, the responsivity decreases approximately as P^{-1}. The last observation is in agreement with that of Ref. [23], where it was found that $R \propto P^{-1+\beta}$ with $\beta = 0.0043$. Analogous results were obtained for ZnO QDs on graphene [28]. Responsivity was found to be constant up to the irradiations of 10^{-8} W/cm^2 and decreases as P^{-1} at higher power. In Ref. [28], the observed dependence was associated with the dependence of photoelectron lifetime on power,

$$\tau_l = \frac{\tau_l(0)}{1 + P/P_0}, \tag{12}$$

and corresponding decrease in the photoconductive gain with power. The power independent responsivity at small power and dependence $R \propto P^{-1}$ at higher power were also observed in Ref. [65] for PbSe-graphene phototransistor and in Ref. [36] for PbS-graphene phototransistor. Finally, in Ref. [68], it has been demonstrated that the field-enhanced charger transfer from PbS QDs to graphene via additional ITO electrode drastically increases the power range (up to 10^{-3} W/cm^2), where the responsivity is power independent (see Figure 9D).

Let us note that different results were obtained in PbS QD-graphene phototransistor in Ref. [10] (Figure 9B) and for phototransistors with WS_2 [17], SnS_2 [8], and MoS_2 [21] channels. The corresponding values of the exponent β in the dependence $R \propto P^{-1+\beta}$ are summarized in Table 2. As seen, while for the graphene phototransistors, exponent β was found close to zero, for WS_2, SnS_2, and MoS_2 phototransistors, the values of β are substantially different from zero.

The dependence $R \propto P^{-1}$ observed at high powers in graphene transistors shows that the photogeneration rate or photocarrier transfer from QDs to graphene is independent of power. In our opinion, this observation cannot be explained by the absorption saturation in the QD nanomaterial or saturation of bipolar tunneling at high powers, which were proposed in the original works. The saturation of the QD absorption or bipolar tunneling would require substantially larger power.

In our opinion, the bottleneck in the phototransistor operation at high power is determined by the finite states available for photocarriers in graphene. The number of

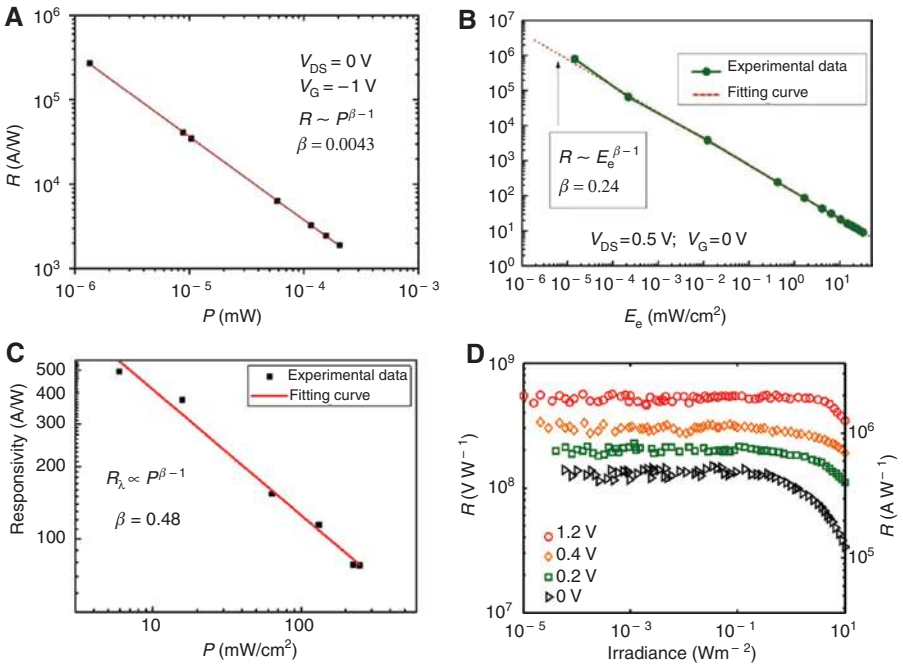

Figure 9: Responsivity vs. electromagnetic power: the graphene transistors with PbS QDs with different ligands (A) [23], (B) [10], and (C) [62]; (D) integrating diode-transistor detector based on graphene with PbS QDs [68].

such states is proportional to the electron density of states in graphene

$$\mathrm{DOS}(\varepsilon) = 8\pi\varepsilon/(h v_F)^2, \tag{13}$$

where $v_F = 5\times10^8$ cm/s is the Fermi velocity in graphene. The characteristic energy interval of photoelectron transfer is ~3 kT, and the number of available states may be evaluated as DOS(ε)·3kT. Then the characteristic power is given by

$$P_0 = \frac{3kT\cdot \mathrm{DOS}(\varepsilon)\,h\nu}{\tau_\ell}. \tag{14}$$

Thus, the characteristic power strongly depends on the photoelectron lifetime and weakly depends on the device band structure (work functions of materials and doping) via the linear energy dependence of DOS. For typical values $\varepsilon \sim 0.5$ eV and $\tau_\ell = 1$ s, we evaluate P_0 as 10^{-8} W/cm², which is in agreement with the experimental observations. The proposed model also predicts that for devices with short photocarrier lifetime, the characteristic power is shifted to higher values. This is confirmed by the data of Ref. [68], where τ_ℓ was evaluated as 10^{-4} s and P_0, as 10^{-4} W/cm² (see Figure 9D). Thus, the short photoelectron lifetime substantially increases the characteristic power and the dynamic range of the detector.

In general, charge transfer from QDs to graphene is determined by two processes. The first one is the diffusion of photocarriers in QD nanomaterial to the relatively narrow depletion region, where under electric field, the photocarriers drift to the channel. The width of the depletion area, L_{dp}, depends on doping of QD structure and graphene and also by the number of electron (hole) states in the 2D materials. Because of the small number of states, the depletion length is small. The characteristic time of the drift charge transfer, $\tau_{dp} = L_{dp}/(\mu E) \approx L_{dp}^2/(\mu V_g)$, depends on the electric field (gate voltage). As the depletion length is small, at any reasonable gate voltage, the drift processes are significantly shorter than the diffusion time in the QD structure,

$$\tau_{dif} = \frac{1}{\pi^2}\frac{L_{QD}^2}{D}, \tag{15}$$

where L_{QD} is the length of the QD material and D is its diffusion coefficient. Thus, the bottleneck in the charge transfer to graphene critically depends on the diffusion process in the QD nanomaterial. If the characteristic diffusion time, τ_{dif}, exceeds the recombination time, τ_R, the diffusion processes are accompanied by the recombination losses in the QD structure. The diffusion-recombination processes decrease the responsivity and increase the exponent β above zero ($\beta = 0$ is expected for the ideal device).

As it was discussed in Section 2, the diffusion coefficient exponentially decreases with the increase in the ligand length (see Table 1). In particular, ligands of the amine group are relatively long, and even in the QD nanomaterial

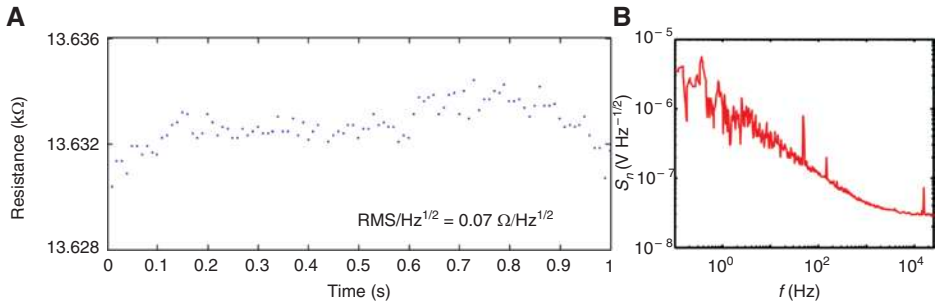

Figure 10: Noise characteristics of the hybrid detectors: (A) Fluctuations of the channel resistance in the graphene transistors with PbS QDs [7]; (B) noise vs. the modulation frequency in the integrating diode-transistor detector [68].

with the shortest amine ligand, pyridine, the electron and hole mobilities are below 10^{-4} cm^2/s·V [24]. The corresponding diffusion coefficient is below 3×10^{-6} cm^2/s, and for typical 100-nm length of QD structure, the diffusion time is above 3 μs, which exceeds the typical recombination time, $\tau_R \sim 0.1$ μs, in PbS QD nanomaterial [52]. This explains the increase of β to 0.24 observed in hybrid transistors based PbS QDs capped with pyridine ligands [10] (see Table 2). Use of shorter ligands enhances photoresponse and reduces the recombination losses. In comparison with the QDs-graphene phototransistors, most of WS_2, SnS_2, and MoS_2 hybrid devices show substantially weaker photoresponse and significantly higher values of β (see Table 2), which are interrelated as we discussed above. In our opinion, the strong advantage of graphene for use in hybrid phototransistors is the continuous density of electron states, which does not need precise level alignment with the QD nanomaterial. Hybrid phototransistors based on 2D materials having a semiconductor bandgap require accurate band engineering to match the electron levels of QDs, 2D conductors, and ligands that provide electron coupling between QDs and 2D channel. The potential advantage of 2D bandgap materials is the expected low dark current and corresponding noise currents.

5.5 Noise and sensitivity

The detector performance is determined by the signal-to-noise ratio, which is given by noise equivalent power (Eq. 4). Unfortunately, the noise characteristics of hybrid transistors were measured only in a few papers [7, 21, 68]. At the same time, the noise measurements have been carried out in detectors with graphene [7] and MoS_2 [21] channels and also in the diode-transistor integrating detector [68] (see Figure 10), which allows us to compare various materials and detector designs. The noise characteristics and sensitivities of the detectors are summarized in Table 3. First of all, it is interesting to compare graphene and MoS_2 transistors. Graphene has substantially higher mobility and, therefore, the photoconductive gain and responsivity. While the electron-hole spectrum in graphene is gapless, MoS_2 has a relatively large gap and, therefore, the dark current and the noise currents in MoS_2 are expected to be substantially smaller than the corresponding currents in graphene. As seen from Table 2, the hybrid graphene-QD structures demonstrate better detectivity at comparable operating times. Thus, the high gain of the graphene-QD transistors provides not only the highest responsivity but also the highest sensitivity of detectors.

The noise mechanisms were investigated in Refs. [21] and [68]. It was found that at low modulation frequencies, 1–1000 Hz, the $1/f$ noise dominates over other noise mechanisms in the fluctuations of the dark current. In Ref. [21], the measured noise was compared with the shot noise, which was considered by the authors as a fundamental limit for sensitivity in hybrid transistors. They have found that at low frequencies, the $1/f$ noise in the MoS transistors exceeds by 10^3–10^4 times the shot noise.

Table 3: Noise characteristics of hybrid phototransistors.

	Responsivity A/W	Noise	NEP W·Hz$^{-1/2}$	Detectivity Jones	Characteristic time (s)	Ref.
PbS QDs – Graphene	$5\cdot10^7$	0.1 Ω/Hz$^{1/2}$	10^{-17}	7×10^{13}	~1	[7]
PbS QDs – MoS_2	$6\cdot10^5$	$(0.6–10)\times10^{-9}$ A/Hz$^{1/2}$ at $f=1$ Hz	7×10^{-16}	5×10^{11}	0.3–0.4	[21]
ITO-PbS QDs-Graphene	10^6	2.5×10^{-8} V/Hz$^{1/2}$	0.6×10^{-15}	1×10^{13}	~10^{-4}	[68]

In our opinion, the fundamental limit of the sensitivity of the high-gain hybrid phototransistors is determined by the "generation-recombination" noise, where the number of photocarriers in the channel fluctuates due to the capture of photocarriers from the channel to the QDs and the inverse process of photocarrier generation from QDs to the channel. According to Eqs. 1–4, for $\gamma >> 1$, we can derive a simple relation between NEP, the dark current, J_{dc}, and responsivity, R,

$$\mathrm{NEP} = 2\sqrt{\frac{J_{dc}}{R}}\sqrt{\frac{h\nu}{\eta}}. \tag{16}$$

In the case, when the short noise dominates over the GR noise, the corresponding noise equivalent power, $\mathrm{NEP} = 2\sqrt{eJ}/R$, is $\sim\gamma^{1/2}$ times smaller than that in the high gain GR limit. However, in current hybrid phototransistors, the $1/f$ noise dominates over both the GR noise and shot noise.

5.6 Photodetector integrated QD diode with graphene transistor

As discussed in the previous section, the main problem of the hybrid QD-2D conductor transistors is the relatively long (1–0.1 s) operating time and corresponding short bandwidth. Slow operation puts strong limitations on applications of hybrid transistors in multi-elements sensing and imaging technologies. Also, intrinsic $1/f$ noise as well as $1/f$ noise of electronic circuits strongly reduces the sensitivity of detectors. As we discussed in Section 4.4, the bottleneck in the charge transfer from QD structure to graphene is determined by the diffusion processes in QD material. To accelerate the operation of hybrid phototransistors, in Ref. [68], a device architecture with additional indium tin oxide (ITO) top-contact, which covered the PbS QD nanomaterial, was proposed and experimentally investigated. Thus, the circuit ITO-QDs-graphene forms a diode structure that is combined with the graphene transistor. The ITO-graphene voltage accelerates photocarriers and modifies slow diffusion processes in the QD structure to fast drift charge transfer. This architecture strongly reduces the operating time, to ~0.1 ms, which, in turn, allows the authors to overcome the $1/f$ noise at operating frequencies.

The voltage responsivity, $R_v = 4\times10^7$ V/W, and noise voltage, $V_n = 2.5\times10^{-8}$ V/Hz$^{1/2}$, measured in Ref. [68] result in the noise equivalent power of $\mathrm{NEP} = V_n/R_v = 0.6\times10^{-15}$ W/Hz$^{1/2}$. Let us analyze the photodetector sensitivity in terms of high-gain generation recombination noise. Substituting into Eq. (16), the current responsivity $R = 10^6$ A/W and the dark current $J_{dc} = 100$ μA, we will find the NEP value of 0.6×10^{-15} W/Hz$^{1/2}$ in agreement with the directly measured results. Thus, the integrating QD diode-graphene transistor device architecture allows for achieving the fundamental limit of sensitivity determined by generation recombination processes in high gain devices.

6 Summaries and outlook

This article reviews emerging detector technologies based on nanostructures that combines QDs with high mobility 2D conductors. This unique combination of 0D-2D nanomaterials offers an excellent perspective for development of low-cost phototransistors with high gain, selective photoresponse, MHz electronic bandwidth, and high sensitivity in the visible and shortwave infrared ranges. During the last 5 years, the hybrid devices have come a long way from complex studies of detection mechanisms and related optoelectronic phenomena to the developing technology for numerous sensing and imaging applications. Intensive investigations of hybrid structures include a variety of QD optoelectronic nanomaterials (PbS, PbSe, ZnO, etc.) and 2D materials (graphene, WS_2, MoS_2, etc.). In this review, we discussed advanced fabrication methods, physical mechanisms of photoresponse, and basic parameters of photodetectors. The comparative analysis of various hybrid phototransistors and comparison of experimental device characteristics with theoretical models provide a better understanding of current achievements and further perspectives in this very promising area. The following paragraphs will provide a brief summary of the main requirements for QD materials, 2D materials, and device architecture and discuss possible steps for further optimization of these devices.

The main requirements to the QD nanomaterial for application in hybrid phototransistors are high resonance absorption, which leads to photocarrier generation, and high photocarrier diffusion, which provides fast charge transfer from the QD structure to the graphene. Currently, it is well understood that the diffusion coefficient exponentially increases with decreasing the ligand length [26]. Use of QD nanomaterial with short ligands significantly reduces recombination losses, increases the photoresponse, and simultaneously increases the operating rate. While in the current phototransistors the mobility of the QD structures does not exceed 0.1 cm^2/s (see Tables 1 and 2), recent

progress in nanoscale engineering of QD nanomaterials with short ligands has improved mobility above 10 cm^2/s [70]. These achievements provide a solid base for further improvement of hybrid phototransistors. Direct relation of the transistor spectral characteristic with QD absorption is experimentally established and well understood. The absorption theory [48] gives a direct relation between the resonance absorption of QDs and the rate of photocarrier escape from the excited QD states (Eqs. 6 and 7). This interrelation of absorption and mobility allows for further optimization of parameters of QD nanomaterial and its thickness. To the best of our knowledge, this effect has not yet been experimentally investigated. Also, systematic studies of the phototransistor characteristics as a function of QD doping would be very useful for understanding charge photogeneration and its transfer in QD structures.

Considering 2D materials for hybrid phototransistors, it is interesting to compare graphene with 2D semiconductors. Graphene has substantially higher mobility, which leads to high gain and high photoresponse. Due to a large bandgap, the 2D semiconductor materials demonstrate substantially lower dark current and, therefore, the better noise characteristics may be expected. As it is shown in Tables 2 and 3, currently, the graphene-based hybrid transistors substantially surpass 2D semiconductor devices in responsivity, sensitivity, and operating rate. In our opinion, the key advantage of graphene lies in its universality. The optoelectronic QD-graphene nanostructures do not need fine level alignment, which is required for matching QD levels to the conducting (valence) band in the bandgap semiconductor. At the same time, the small density of electron states in graphene (Eq. 13) leads to the relatively small dark current and, therefore, small noise equivalent power (Eq. 4).

In this work, we have developed a model that well describes the dependence of the responsivity on the electromagnetic power for a graphene transistor and determined the characteristic power, P_0, below at which the photoresponse is linear in power (Eq. 14). As the characteristic power is proportional to the DOS in graphene and the noise current is proportional to $DOS^{1/2}$, the detector dynamic range is proportional to $DOS^{1/2}$ and it may be effectively controlled by the gate voltage. The gate control of operating regimes opens intriguing possibilities for adaptive sensing.

Complex optimization of the transistor design provides significant room for improvements of all detector parameters. First of all, the well-developed solar cell methods for light trapping [50] may be applied to the phototransistors for enhancement of QD absorption and reduction of QD nanomaterial thickness, which, in turn, is expected to improve the device operating rate. Decrease of the device length will increase the gain and responsivity (Eq. 9). Decrease of the device square (length and width) will improve the noise equivalent power, i.e. sensitivity (Eq. 4). Additional transparent top contact covered QD nanomaterial [68] provides efficient control of the photocarrier transport in QD structure. In this design, the field-induced photoelectron drift strongly accelerates the devices operation. The electronic bandwidth of 1.5 kHz has been already demonstrated [68].

In this work, we have defined the limiting sensitivity of hybrid phototransistors, which is determined by the generation-recombination noise in high gain devices. The corresponding noise equivalent power can be calculated using the measured dark current and responsivity (Eq. 16). We have demonstrated that this limiting sensitivity has been achieved in the recent work [68], where devices integrating QD photodiodes and graphene phototransistors were proposed and investigated. Thus, the hybrid phototransistor technology has already reached some level of maturity, at which the photoresponse and noise mechanism are determined by the same photoelectronic processes, i.e. all additional noise mechanisms are suppressed. This achievement opens possibilities for improvement of the operating rate and sensitivity by operating at modulation frequencies between the photoresponse bandwidth and the noise bandwidth, which is determined by crossing of the generation-recombination noise with an additional noise, for example, in the ideal case with the Jonson noise. In this way, the ultrahigh responsivity of hybrid transistors may be sacrificed for improvement of other critical characteristics.

In conclusion, the hybrid QD-2D channel phototransistors have already demonstrated ultrahigh gain, high efficiency, high sensitivity, and spectral selectivity for operation in the visible and near-IR ranges. Additional gate control of electron transport in QD nanomaterial allows for increase in the operating speed. Fast progress in material science and nanotechnologies provides numerous intriguing possibilities for further improvements of hybrid phototransistors.

Acknowledgments: The authors wish to acknowledge Dr. John Little for useful discussions. The research was supported by U.S. Army Research Laboratory. AS also acknowledges NRC support. The authors would like to thank all colleagues, whose figures and data were used in this review.

References

[1] Bonaccorso F, Sun Z, Hasan T, Ferrari AC. Graphene photonics and optoelectronics. Nat Photonics 4;2010:611–22.

[2] Liu CH, Chang YC, Norris TB, Zhong Z. Graphene photodetectors with ultra-broadband and high responsivity at room temperature. Nat Nanotechnology 2014;9:273–8.

[3] Mak KF, Ju L, Wang F, Heinz TF. Optical spectroscopy of graphene: from the far infrared to the ultraviolet. Solid State Commun 2012;152:1341–9.

[4] Liu M, Yin X, Ulin-Avila E, et al. A graphene-based broadband optical modulator. Nature 2011;474:64–7.

[5] Lemme MC. Gate-activated photoresponse in a graphene p-n junction. Nano Lett 2011;11:4134–7.

[6] Wilson JA, Yoffe AD. The transition metal dichalcogenides discussion and interpretation of the observed optical, electrical and structural properties. Adv Phys 1969;18:193–335.

[7] Konstantatos G, Badioli M, Gaudreau L, et al. Hybrid graphene-quantum dot phototransistors with ultrahigh gain. Nature Nanotechnol 2012;7:363–8.

[8] Huang Y, Zhan X, Xu K, et al. Highly sensitive photodetectors based on hybrid 2D-0D SnS2-copper indium sulfide quantum dots. Appl Phys Lett 2016;108:013101.

[9] Robin A, Lhuillier E, Xu XZ, et al. Engineering the charge transfer in all 2D graphene-nanoplatelets heterostructure photodetectors. Sci Rep 2016;6:24909.

[10] Sun ZH, Liu ZK, Li JH, Tai GA, Lau SP, Yan F. Infrared photodetectors based on CVD-grown graphene and PbS quantum dots with ultrahigh responsivity. Adv Mater 2012;24:5878–83.

[11] Gao S, Dong S. Graphene nanosheet: synthesis, molecular engineering, thin film, hybrids, and energy and analytical applications. Chem Soc Rev 2011;40:2644 –72.

[12] Bhimanapati GR, Linǫ Z, Meunier V, et al. Recent advances in two dimensional materials beyond graphene. ACS Nano 2015;9:11509–39.

[13] Zhang Y, Zhang L, Zhou C. Review of chemical vapor deposition of graphene and related applications. Acc Chem Res 2013;46:2329–39.

[14] Bae S, Kim H, Lee Y, et al. Roll-to-roll production of 30-inch graphene films for transparent electrodes. Nat Nanotechnol 5;2010:574–8.

[15] Nicolosi V, Chhowalla M, Kanatzidis MG, Strano MS, Coleman JN. Liquid exfoliation of layered materials. Science 2013;340:1226419.

[16] Schornbaum J, Winter B, Schießl SP, et al. Epitaxial growth of PbSe quantum dots on MoS2 nanosheets and their near-infrared photoresponse. Adv Funct Mater 2014;24:5798–806.

[17] Jia Z, Xiang J, Wen F, Yang R, Hao C, Liu Z. Enhanced photoresponse of SnSe-nanocrystals-decorated WS2 monolayer phototransistor. ACS Appl Mater Interfaces 2016;8:4781–8.

[18] Chen K, Wan X, Wen J, et al. Electronic properties of MoS2–WS2 heterostructures synthesized with two-step lateral epitaxial strategy. ACS Nano 2015;9:9868–76.

[19] Iler R. Multilayers of colloidal particles. J Colloidal Interface Sci 1966;21:569–94.

[20] Watanabe E, Spidle R, Caudle S, Manani G, Wanekaya AK, Mugweru A. Electrochemical method for analysis of cholesterol based on in situ synthesized graphene decorated with zinc oxide nanoparticles. ECS Solid State Lett 2001;3:M5–9. 10.1149.

[21] Kufer D, Nikitskiy I, Lasanta T, Navickaite G, Koppens FHL, Konstantatos G. Hybrid 2D–0D MoS 2–PbS quantum dot photodetectors. Adv Mater 2015;27:176–80.

[22] Kim BS, Neo DCJ, Hou Bo, et al. High performance PbS quantum dot/graphene hybrid solar cell with efficient charge extraction. ACS Appl Mater Interfaces 2016;8:13902–8.

[23] Wang R, Zhang YT, Wang HY, Song XX, Jin LF, Yao JQ. Wide spectral response field effect phototransistor based on graphene-quantum dot hybrid. IEEE Photonics 2015;7:450076.

[24] Hetsch F, Zhao N, Kershaw SV, Rogach AL. Quantum dot field effect transistors. Mater Today 2016;16:9.

[25] Zhang Y, Cao M, Song X, et al. Multiheterojunction phototransistors based on graphene–PbSe quantum dot hybrids. J Phys Chem C 2015;119:21739–43.

[26] Liu Y, Gibbs M, Puthussery J, et al. Dependence of carrier mobility on nanocrystal size and ligand length in PbSe nanocrystal solids. Nano Lett 2010;10:1960–9.

[27] Gao Y, Aerts M, Sandeep CS, et al. Photoconductivity of PbSe quantum- dot solids: dependence on ligand anchor group and length. ACS Nano 2012;6:9606–14.

[28] Guo WH, Xu SG, Wu ZF, Wang N, Loy MMT, Du SW. Oxygen-assisted charge transfer between ZnO quantum dots and graphene. Small 2013;9:3031–6.

[29] Xu F, Gerlein LF, Ma X, Haughn CR, Doty MF, Cloutier SG. Impact of different surface ligands on the optical properties of PbS quantum dot solids. Materials 2015;8:1858–70.

[30] Abel KA, Shan J, Boyer JC, Harris F, van Veggel FCJM. Highly photoluminescent PbS nanocrystals: the beneficial effect of trioctylphosphine. Chem Mater 2008;20:3794–6.

[31] Cuharuc AS, Kulyuk LL, Lascova RI, Mitioglu AA, Dikusar AI. Electrochemical characterization of PbS quantum dots capped with oleic acid and PbS thin films – a comparative study. Surface Eng Appl Electrochem 2012;48:3.

[32] Dubois F, Mahler B, Dubertret B, Doris E, Mioskowski CA. Versatile strategy for quantum dot ligand exchange. J Am Chem Soc 2007;129:482–3.

[33] Jeong KS, Tang J, Liu J, et al. Enhanced mobility-lifetime products in PbS colloidal quantum dot photovoltaics. ACS Nano 2012;6:89–99.

[34] Luther JM, Law M, Song Q, Perkins CL, Beard MC, Nozik AJ. Structural optical, and electrical properties of self-assembled films of PbSe nanocrystals treated with 1,2-ethanedithiol. ACS Nano 2008;2:271–80.

[35] Talapin DV, Murray CB. PbSe nanocrystal solids for n- and p-channel thin film field-effect transistors. Science 2005;310:86–9.

[36] Turyanska L, Makarovsky O, Svatek SA, et al. Ligand-induced control of photoconductive gain and doping in a hybrid graphene–quantum dot transistor. Adv Electron Mater 2015;1:1500062.

[37] Zhang H, Hu Bo, Sun L, et al. Surfactant ligand removal and rational fabrication of inorganically-connected quantum dots. Nano Lett 2011;11:5356–61.

[38] Konstantatos G, Sargent EH. Colloidal quantum dot optoelectronics and photovoltaics. New York: Cambridge University Press, 2013.

[39] Gao J, Nguyen SC, Bronstein ND, Alivisatos AP. Solution-processed, high-speed, and high-quantum-efficiency quantum dot infrared photodetectors. ACS Photonics 2016;3:1217–22.

[40] Efros Alexander L, Efros Alexei L. Interband absorption of light in a semiconductor sphere. Sov Phys Semicond 1982;16:772–5.

[41] Moreels I, Lambert K, Smeets D, et al. Size-dependent optical properties of colloidal PbS quantum dots. ACS Nano 2009;3:3023–30.
[42] Moreels I, Lambert K, De Muynck D, et al. Composition and size-dependent extinction coefficient of colloidal PbSe quantum dots. Chem Mater 2007;19:6101–6.
[43] Allan G, Delerue C. Confinement effects in PbSe quantum wells and nanocrystals. Phys Rev B 2004;70:245321.
[44] Lin KF, Cheng HM, Hsu HC, Lin LJ, Hsieh WF. Band gap variation of size-controlled ZnO quantum dots synthesized by sol–gel method. Chem Phys Lett 2005;409:208–11.
[45] Kamat PV. Quantum dot solar cells. Semiconductor nanocrystals as light harvesters. J Phys Chem C 2008;112:18737–53.
[46] McDonald SA, Konstantatos G, Zhang S, et al. Solution-processed PbS quantum dot infrared photodetectors and photovoltaics. Nat Mater 2005;4:138–42.
[47] Nozik AJ. Quantum dot solar cells. Physica E 2002;14:115–20.
[48] Lang IG, Pavlov ST. Resonant light absorption by semiconductor quantum dots. Adv Condens Matter Phys 2009;2009:645190.
[49] Yablonovitch E. Inhibited spontaneous emission in solid-state physics and electronics. Phys Rev Lett 1987;58:2059.
[50] Tiedje T, Yablonovitch E, Cody GD, Brooks BG. Limiting efficiency of silicon solar cells. IEEE Trans Electron Devices 1984;31:711–6.
[51] Schaller RD, Klimov VI. High efficiency carrier multiplication in PbSe nanocrystals: implications for solar energy conversion. Phys Rev Lett 2004;92:186601.
[52] Ellingson RJ, Beard MC, Johnson JC, et al. Highly efficient multiple exciton generation in colloidal PbSe and PbS quantum dots. Nano Lett 2005;5:865–71.
[53] Sukhovatkin V, Hinds S, Brzozowski L, Sargent EH. Colloidal quantum-dot photodetectors exploiting multiexciton generation. Science 2009;324:1542–4.
[54] Konstantatos G, Howard I, Fischer A, et al. Ultrasensitive solution-cast quantum dot photodetectors. Nature 2006; 442:180–3.
[55] Adinolfi V, Sargent EH. Colloidal quantum dot photodetectors. Proc. SPIE 9555, Optical Sensing, Imaging, and Photon Counting: Nanostructured Devices and Applications, 955506, 2015.
[56] Beneking H. Gain and bandwidth of fast near-infrared photodetectors: a comparison of diodes, phototransistors, and photoconductive devices. IEEE Trans Electron Devices 1982;29:1420–31.
[57] Ogura M. Hole injection type InGaAs–InP near infrared photo-FET, IEEE J. Quantum Electron 2010;46:562–9.
[58] Mitin VV, Pipa VI, Sergeev AV, Dutta M, Stroscio M. High-gain quantum-dot infrared photodetector. Infrared Phys Technol 2001;42:467–72.
[59] Mitin V, Antipov A, Sergeev A, Vagidov N, Eason D, Strasser G. Quantum dot infrared photodetectors: photoresponse enhancement due to potential barriers. Nanoscale Res Lett 2011;6:21.
[60] Martyniuk P, Rogalski A. Quantum-dot infrared photodetectors: status and outlook. Prog Quantum Electron 2008;32:89–120.
[61] Zhang DY, Gan L, Cao Y, Wang Q, Qi LM, Guo XF. Understanding charge transfer at PbS-decorated graphene surfaces toward a tunable photosensor. Adv Mater 2012;24:2715–20.
[62] Huang YQ, Zhu RJ, Kang N, Du J, Xu HQ. Photoelectrical response of hybrid graphene PbS quantum dot devices. Appl Phys Lett 2013;103:143119.
[63] Wang R, Zhang YT, Wang HY, et al. High-performance controllable ambipolar infrared phototransistors based on graphene – quantum dot hybrid. Arxiv Condmat 2014;arXiv:1410.2413v1.
[64] Son DI, Yang HY, Kim TW, Park WI. Photoresponse mechanisms of ultraviolet photodetectors based on colloidal ZnO quantum dot graphene nanocomposites. Appl Phys Lett 2013;102:021105.
[65] Song X, Zhang Y, Zhang H, et al. Improved photoelectronic performance of graphene, polymer and PbSe quantum dot infrared photodetectors. Mater Lett 2016;178:52–5.
[66] Kufer D, Konstantatos G. Highly sensitive, encapsulated MoS2 photodetector with gate controllable gain and speed. Nano Lett 2015;15:7307–13.
[67] Liu X, Liu N, Liu M, et al. Graphene nanomesh photodetector with effective charge tunnelling from quantum dots. Nanoscale 2015;7:4242–9.
[68] Nikitskiy I, Goossens S, Kufer D, et al. Integrating an electrically active colloidal quantum dot photodiode with a graphene phototransistor. Nat Commun 2016;7:11954.
[69] Adinolfi V, Kramer IJ, Labelle AJ, Sutherland BR, Hoogland S, Sargent EH. Photojunction field-effect transistor based on a colloidal quantum dot absorber channel layer. ACS Nano 2015;9:356–62.
[70] Zhitomirsky D, Voznyy O, Levina L, et al. Engineering colloidal quantum dot solids within and beyond the mobility-invariant regime. Nat Commun 2014;5:3803.